Nanoscale

Accepted Manuscript

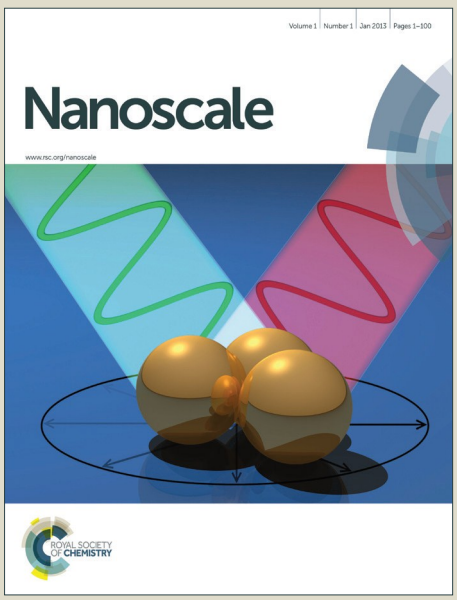

ROYAL SOCIETY OF CHEMISTRY

www.rsc.org/nanoscale

Nanoscale

RSCPublishing

COMMUNICATION

Controlled manipulation of Fe_3O_4 nanoparticles in an oscillating magnetic field for fast ablation of microchannel occlusions

Cite this: DOI: 10.1039/xoxxoooooox

Received ooth October 2014,
Accepted ooth October 2014

DOI: 10.1039/xoxxoooooox

www.rsc.org/

Jacque Lynn F. Gabayno, *[a,b] Da-Wei Liu,[c] Ming Chang,*[a,c] and Yu-Hao Lin[c]

Fe_3O_4 nanoparticles were controlled by oscillating magnetic field to enable fast and non-contact ablation of microchannel occlusions. Scalable behaviour of their translation and rotational velocities were experimentally verified. Rotational flows created by such motions are fundamental for ablation as demonstrated by the removal of thrombus in occluded microchannel.

Development of magnetic materials with dimensions ranging from a few nanometers to several micrometers sparks many opportunities for biomedical, nanotechnology, and bioengineering applications [1-3]. Biocompatible magnetic nanomaterials, which are currently being used as contrast agents in imaging systems, are also envisioned for controlled drug delivery systems, cell labelling/sorting, and minimally invasive nano/microsurgery tools [4, 5]. The obvious benefits of employing extremely small materials for laboratory diagnostics and therapeutics include the straightforward delivery of the nano/microparticles through the bloodstream as well as target-specific treatment of abnormal tissues/organs.

Iron oxide-based nanomaterials, such as maghemite (γ-Fe_2O_3) and magnetite (Fe_3O_4), are reported to exhibit superparamagnetic properties at room temperature [6-9]. These materials are strongly magnetized by an external magnetic field, permitting stable and local interaction with potential target structures (e.g. cancer cells, tumors, blood cells, emboli, and lipomas). Controlled operation and functionalization for binding with physiological structures are being highlighted to complement their biocompatibility [10-12]. Various means of control mechanism are proposed to offset the inherent difficulty of moving extremely small particles. Autonomous motion strategies through chemical reactions, ultrasonic propulsion, and thermophoresis have been developed [13-18]. External forces from magnetic and electric field sources are similarly explored [19-26]. In this report, we investigate the motion behaviour of iron (II, III) oxide (Fe_3O_4) nanoparticles using an oscillating magnetic field.

Magnetic nanoparticles such as Fe_3O_4 acquire large dipole moments when immersed in an external magnetic field, which consequently align the particles with the magnetic source. Strong dipolar interaction between the magnetized nanoparticles could result to agglomeration, forming chains or rod-like microstructures [27-29]. The agglomerates may unfold as randomly dispersed nanoparticles upon removal of the external field. The reversibility of the clustering behavior has found applications in magnetophoretic separation systems such as in waste water treatment [30]. Our work exploits this known phenomenon to develop microrod structures that move in two or three-dimensional space with a well-defined velocity under an external gradient source. As such, steering microrods towards a target becomes relatively easy because their trajectory is determined by the gradient field. Furthermore, the use of an oscillating magnetic field induces a magnetic torque for the controllable rotation of the microrod. The trajectory, velocity and length of the microrods are found to be mostly dependent on the applied field and, hence, a simple manipulation platform is built to control their movement. Hydrodynamic forces resulting from the rotational motion is used for the non-contact removal of occlusions (e.g. blood clot) in a microchannel.

As shown in Fig. 1a, the construction of the manipulation platform combines a permanent magnet to assemble the nanoparticles into microrods and an electromagnet (solenoid) to produce the oscillating and magnetic field gradient sources for rotation and translation, respectively. Fe_3O_4 nanoparticles were batched prepared in deionized water to make sure that each trial set uses the same concentration of magnetized particles. Initially, the suspension was injected in a narrow glass container to observe the formation of the microrods in real-time. The nanoparticles are randomly dispersed, forming microclusters of varied shapes (Fig. 1b). By positioning the permanent magnet a few centimeters from the tank, the nanoparticles are instantaneously assembled to form rod-like agglomerates (Fig. 1c). Removing the magnet completely

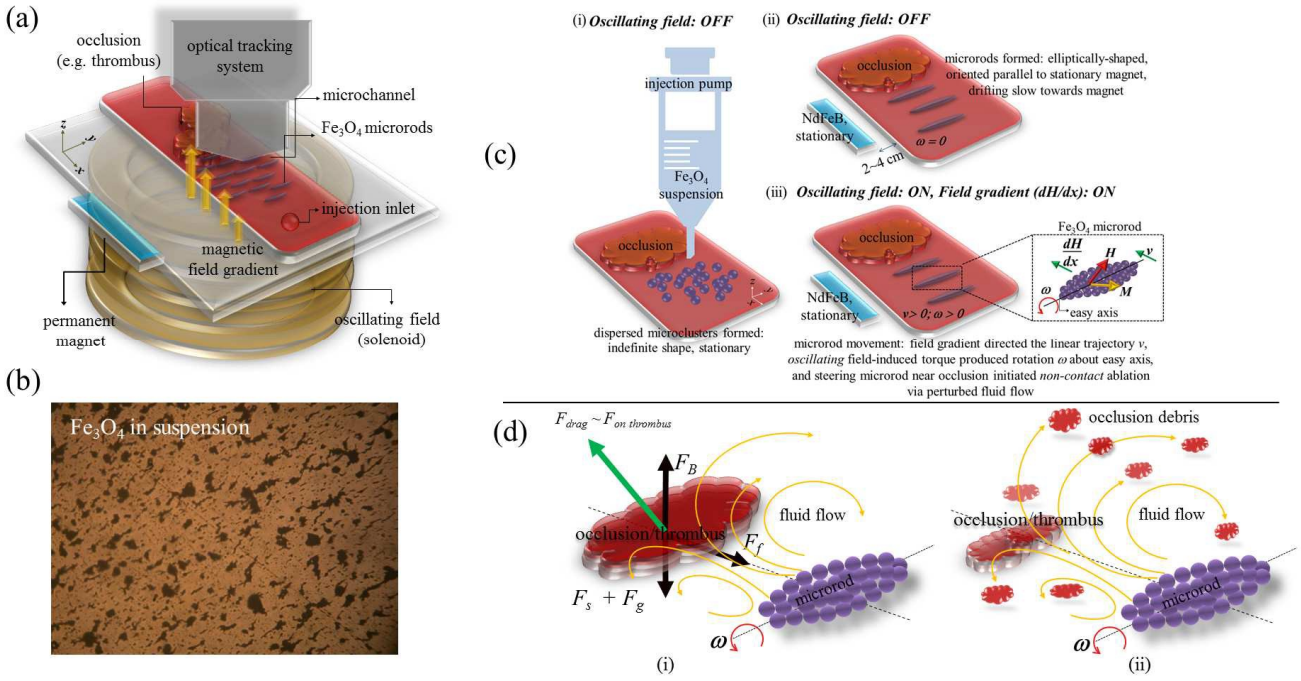

Fig. 1 (a) Fe_3O_4 nanoparticles in suspension form agglomerates of micrometer-size structures. (b) Schematic diagram of magnetic manipulation platform. (c) Control system of nanoparticle movement, their orientation, and motion tendency (i)-(ii) without and (iii) with external oscillating magnetic field. (d) Non-contact removal process of thrombus/occlusion by rotational flow field around rotating microrod. Smaller debris discarded from initial ablation is propelled through the fluid flow and engaged by trailing microrods for complete ablation.

destroys the microrods such that the particles are returned to their initial dispersed state.

The movement of the microrods in the magnetic manipulation platform is controlled by the oscillating field. The general trajectory is determined by the steepest gradient. The rotation chirality is also determined by the coil position with respect to the container tank. Using this configuration, maneuvering the microrods inside the container was easily permitted by translating the coil along the x-y plane.

Observations with various positions and amplitude of the oscillating field were recorded. These observations can be summarized as follows**:** Microrod agglomerates are formed immediately after injection of the Fe_3O_4 nanoparticles into the microchannel. The microrods are elongated and elliptical in shape with long axis aligned parallel to the stationary magnetic field. The magnetization vector *M* is diametric and**,** hence, the rotation tendency is about the long axis. The length and diameter of the microrods are dependent on the magnetic field strength, which can be controlled by tuning the amplitude of the oscillating field as depicted in Fig. 2. The length of the microrods can also be increased by positioning the permanent magnet closer to the microchannel. There is a quadratic dependence in the length of the microrod and the external field, which implies scalability in the shape and dimension of the microstructures. Nanoparticle clusters that settle on the bottom of the microchannel or container are not assembled into microrods, thus remaining stationary because of dominant surface effects. Although the size distribution of the microrods is inhomogeneous, within our measurement limits and depending on the current amplitude supplied to the solenoid**,** the microrods are observed to move with the same velocity and rotation speed.

Journal Name RSCPublishing

COMMUNICATION

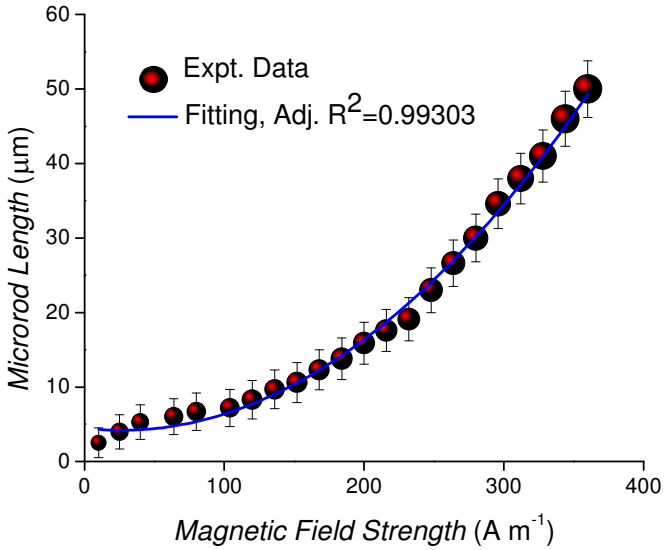

Fig. 2 Microrod length depicts quadratic dependence with magnetic field strength *H*. Fitting parameters: $y = 4.489 - 0.021x + 4.\ 054 \times 10^{-4}\ x^2$.

To establish a generalized formulation for predicting the translation and rotation of the microrods in a viscous fluid, we first assume that the electrostatic and van der Waals forces are negligible. Although in principle, the stability of iron-oxide nanoparticles in the suspension is subjected to attractive van der Waals and hydrophobic effects, the interaction between neighboring clusters is mostly subjected to the strong dipolar interactions in the presence of an external magnetic field (as illustrated in Fig. 1). Moreover, the microrods are observed to be separated by at least one-body length from adjacent microrods, which are also moving closer to the center such that contact with the microchannel wall becomes negligible. Effects from Brownian movement are not immediately observed, thus ruled out from the effective and defined trajectory of the microrod. *(See corresponding ESI Video S1)* Further assuming Newtonian flow throughout the microchannel, the magnetic gradient generated by the coils induces the predominant motive force for the propulsion of the microrods. The magnetic force (F_m) is given by,

$$F_m = \mu_o \chi V \left(\vec{H} \cdot \frac{\Delta \vec{H}}{\Delta x} \right) \qquad (1)$$

where $\mu_0 = 4\pi \times 10^{-7}$ H m^{-1} is the vacuum permeability which is close to that of water, χ (5) is the material susceptibility, V (3 x 10^{-17} m^3) is the volume of the microrod, H is the magnetic field strength, and $\frac{\Delta \vec{H}}{\Delta x}$ is the gradient field.

For non-spherical particles (e.g. chains, fibres, rods), the hydrodynamic Stokes' drag force can be modified according to $F_d = -3\pi L_e \eta f_n v$ where L_e (~4 μm) is the equivalent diameter of a sphere with the same volume as the microrod, η (8.9 x 10^{-4} N • s m^{-2}) is the liquid viscosity, f_n (~2.48) is the dynamic shape correction factor for tightly packed clusters, and v is the linear velocity of the microrod [31-36]. It follows that the velocity of the microrod along the direction of the gradient is,

$$v = \frac{\mu_o \chi V}{3\pi L_e \eta f_n} H \frac{\Delta H}{\Delta x} \qquad (2)$$

Although the microrod may undergo initial acceleration, the time window was too small for accurate tracking measurements. However, the expression in Eq. (2) shows that the terminal velocity should linearly change with the quantity $\left(H \frac{\Delta H}{\Delta x} \right)$, which accounts for the coupled effects of the oscillating magnetic field amplitude and the field gradient. This is experimentally verified in Fig. 3a**,** where the measured velocity from 10 μm s^{-1} to 130 μm s^{-1} linearly increases between the range 2 x 10^9 A^{2}m^{-3}<$\left(H \frac{\Delta H}{\Delta x} \right)$<60 x10^9 A^{2}m^{-3}. The gradient field is measured according to $\frac{\Delta H}{\Delta x} = \frac{H_C - H_E}{x_C - x_E}$ where H_C and H_E correspond to the magnetic field strengths at the center and edge of the container, respectively. Since the magnetic field strength

is not constant, H is approximated to be the average measurement at the center, i.e. $H \cong H_C$.

As discussed above, the rotation of the microrods depends on the interaction of the induced magnetization to the oscillating field. The rotation is on the same plane as the magnetic field (along the *x*-*z* plane in Fig. 1b). If the magnetic dipole moment is represented as $\boldsymbol{m}$ and magnetic induction as $\boldsymbol{B}$, the torque $\boldsymbol{\tau_m}$ on a dipole in free space is determined by the vector product $\vec{\tau}_m = \vec{m} \times \vec{B} = \mu_o \vec{m} \times \vec{H}$. The magnetic dipole moment can be expressed in terms of the magnetization $\boldsymbol{M}$ and the volume of the particle $\vec{m} = \vec{M}V$, which follows that the magnitude of the torque needed to rotate the microrod is,

$$\tau_m = V \frac{\chi^2}{2(2+\chi)} \mu_o H^2 \sin(2\theta) \qquad (3)$$

where θ is the angle between $\boldsymbol{m}$ and $\boldsymbol{B}$. Equation (3) clearly suggests that the magnetic torque will increase with the misalignment angle and volume of the microrods. Most importantly, the expression reveals that the magnetic torque will vary with $|H|^2$.

It should be noted that the actual rotation of the microrods should also account for the viscous drag force. Considering its shape, the induced drag torque on a microrod is given by $\vec{\tau}_D = \frac{16}{3} \pi \eta a b^2 \vec{\omega}$ where a and b are the long and short axes of microrod, respectively, and ω is the rotation speed. In the low Reynolds number regime, the rotating microrods eventually reach terminal velocity instantaneously and the magnetic torque is counterbalanced by the drag torque. As a result, the angular speed is given by,

$$\omega = \frac{3V\chi\mu_o H^2 \sin(2\theta)}{(2+\chi)(32\pi\eta a b^2)} \qquad (4)$$

The expression in Eq. (4) suggests that the rotation of the microrods can be precisely controlled by modulating the oscillating field. It also implies that the motion of the microrods can be stopped or resumed by simply controlling the ac source. It shows further the $|H|^2$ dependence of the rotation speed, which was verified experimentally on a microrod with dimension a = 9 μm and b = 0.9 μm as shown in Fig. 3b.

The driving field frequency in all the measurements was kept at 140 Hz. No significant change in the microrod rotation speed was observed between the full frequency settings of the oscillating source from 40 Hz to 250 Hz. It is supposed that the phase angle between the diametric magnetization of the microrod and the driving field were constant in this frequency range.

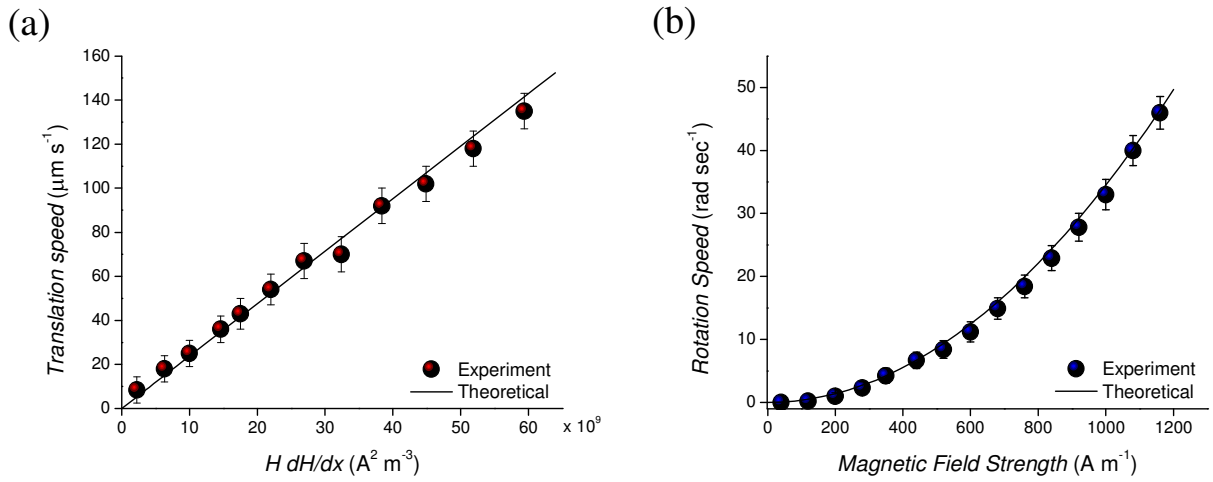

Fig. 3 (a) The microrod velocity reveals a linear dependence to the field gradient $\frac{\Delta H}{\Delta x}$ and magnetic field strength H. (b) Microrod rotation speed shows a nonlinear dependence to H.

The rotation of microrods in a viscous fluid has been shown to create a vortex and rotational flows, which act as a lifting mechanism to move nearby micro-objects in the flow or vortex region [37-40]. Lifting effect is provided by the rotational flow field because of the non-uniform distribution of the flow velocity. In this context, a lifting force can be considered as a fluid drag induced on a nearby object by the rotating microrods (Fig. 1d). A strong rotational flow field can therefore modulate the lift force to overcome the apparent weight of the object as well as adhesion and stiction forces between the object and the contact surface. Such process can be applied to ablate nearby objects to move with the rotational flow. The example reported in this work is the non-contact removal of microchannel occlusions such as a thrombus.

An occlusion in the bloodstream adversely disrupts the supply of oxygen to normal tissues and organs. Traditional treatments use drugs to dissolve the blockage or by surgery using mechanical device that are inserted on the occluded vessel. Our model system used a microchannel with a length of 16 mm and width of 0.8 mm to represent a microvessel [41]. To prepare the thrombus, a drop of blood was injected into the microchannel using a syringe. The blood was obtained from a volunteer by authorized medical staff. It was kept in a vacuum sealed tube and stored in a freezer before the actual experiment. After injection into the microchannel, the blood was

incubated and left to dry at room temperature until a thick and dark layer of solid structures became visible. As shown in Fig. 4a, the opacity of the blood occlusion is higher than the injected Fe_3O_4 nanoparticles, which would indicate that albeit softer than an actual thrombus, the modelled occlusion blocked the circulation of injected fluids completely. The thickness of the thrombus spanned the entire width of the opposing side walls. The nanoparticles were injected (at t = 0 s) on the right side of the microchannel, then maneuvered towards the thrombus area by moving the manipulation platform. The rotation-induced fluid flow by the leading microrods started to ablate the occlusion at t = 5 s until the process created a narrow pathway at the center of the occlusion area (t =15 s). The narrow opening was visibly tapered towards the center of the microchannel, which can be attributed to the non-uniform velocity distribution of the flow field. The thrombus structures near the side walls (indicated by the white arrows) were mostly intact. However, these can be removed completely by translating the coil to re-position the field gradient. The non-contact removal of the central thrombus area was completed in less than 30 seconds using a gradient of 2.54 x 10^6 A m^{-2} and oscillating field strength of 624 A m^{-1}.

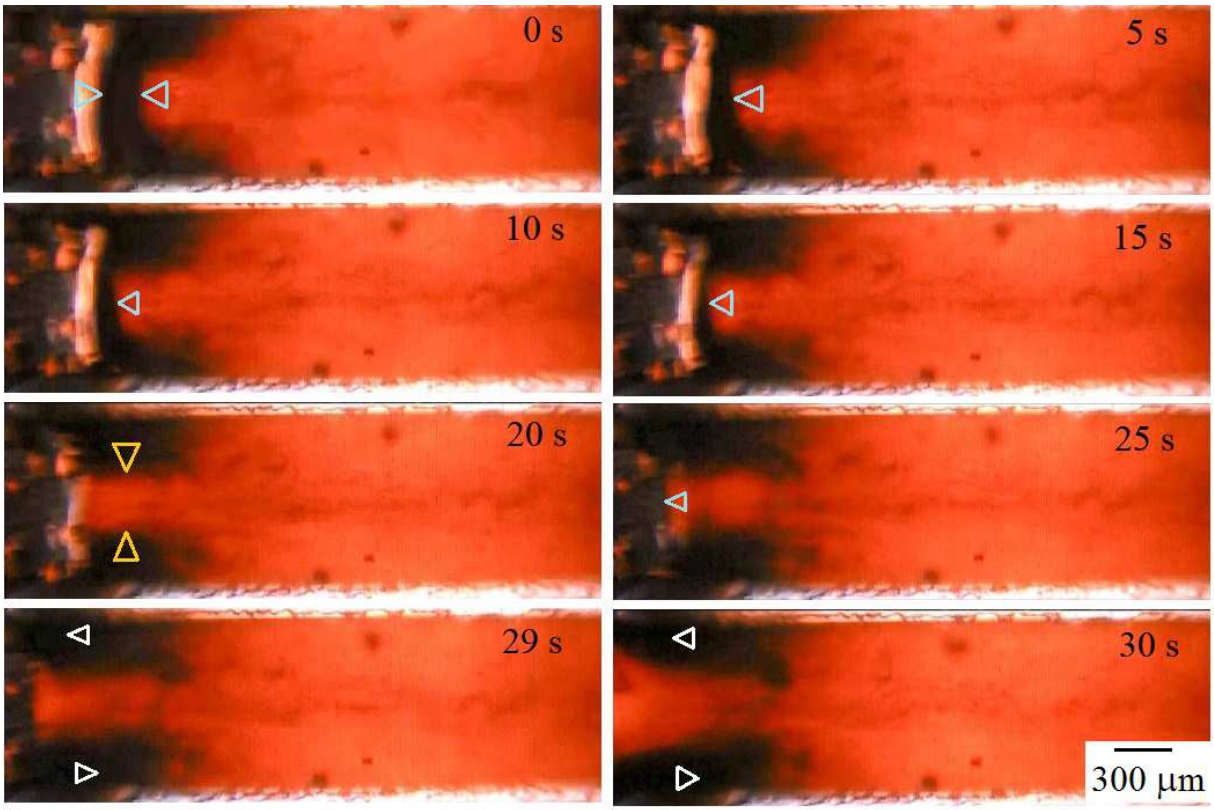

Fig. 4 Image sequence demonstrating the non-contact removal of microchannel occlusion (thrombus) by magnetic steering of Fe_3O_4 microrods; images were captured at 10x magnification. Injection inlet is on the right hand side while the target is indicated by the dense, opaque area on the left (light blue arrow). The yellow arrows indicate the narrow pathway along the centerline of the microchannel after removal of thrombus. The white arrows indicate the occlusion region near the microchannel walls, which remained intact due to the non-uniform velocity distribution in the flow field. *(See corresponding ESI Video S2).*

To inspect the ablation process in more detail, the movement of a single microrod (length of ~200 µm) in the vicinity of the model thrombus was tracked as shown in Fig. 5. First, the oscillating magnetic field was switched on and the permanent magnet was fixed to orient the microrod axis such as shown. Next, the microrod was steered towards the densest occlusion by positioning the solenoid slightly off-center the microscope's field of view. This strategy guides the microrod trajectory towards the steep gradient region shown in Fig. 5a. The microrod rotation was then initiated in the direction shown (Fig. 5b) due to the acquired torque. The hydrodynamic flow field generated by the microrods is also about its rotation axis *(See corresponding ESI Video S3)*, of which the effective drag force from the perturbed velocity field ablates the thrombus without the actual contact to the microrod. Initially static and smaller thrombus structure such as (A) located on the upper left vicinity of the microrod in Fig. 5b was easily ablated by the rotational flow. The structure was propelled through the flow field repeatedly (Fig. 5c) until it was eventually fragmented into tiny debris.

As the microrod moves in the direction of the gradient, the velocity field stimulates faster ablation due to the faster rotation of the microrod, as shown in Fig. 5d-5h. Bigger structures from the occlusion such as (B) and (C) in Fig. 5i-5k were consequently removed and propelled through the fluid flow field until both were totally destroyed or split into smaller structures (Fig. 5l).

In summary, the microrod movement and thrombus ablation were both influenced by the apparent position of the microrod with respect to the field gradient. The relatively slow rotation of the microrod far from the center of the solenoid can only create a weaker velocity field, which also can only destroy smaller structures from a very narrow occlusion area. However, its fast rotation while in motion towards the steep gradient induces stronger velocity field,

which consequently assist in the ablation of bigger structures with more efficiency.

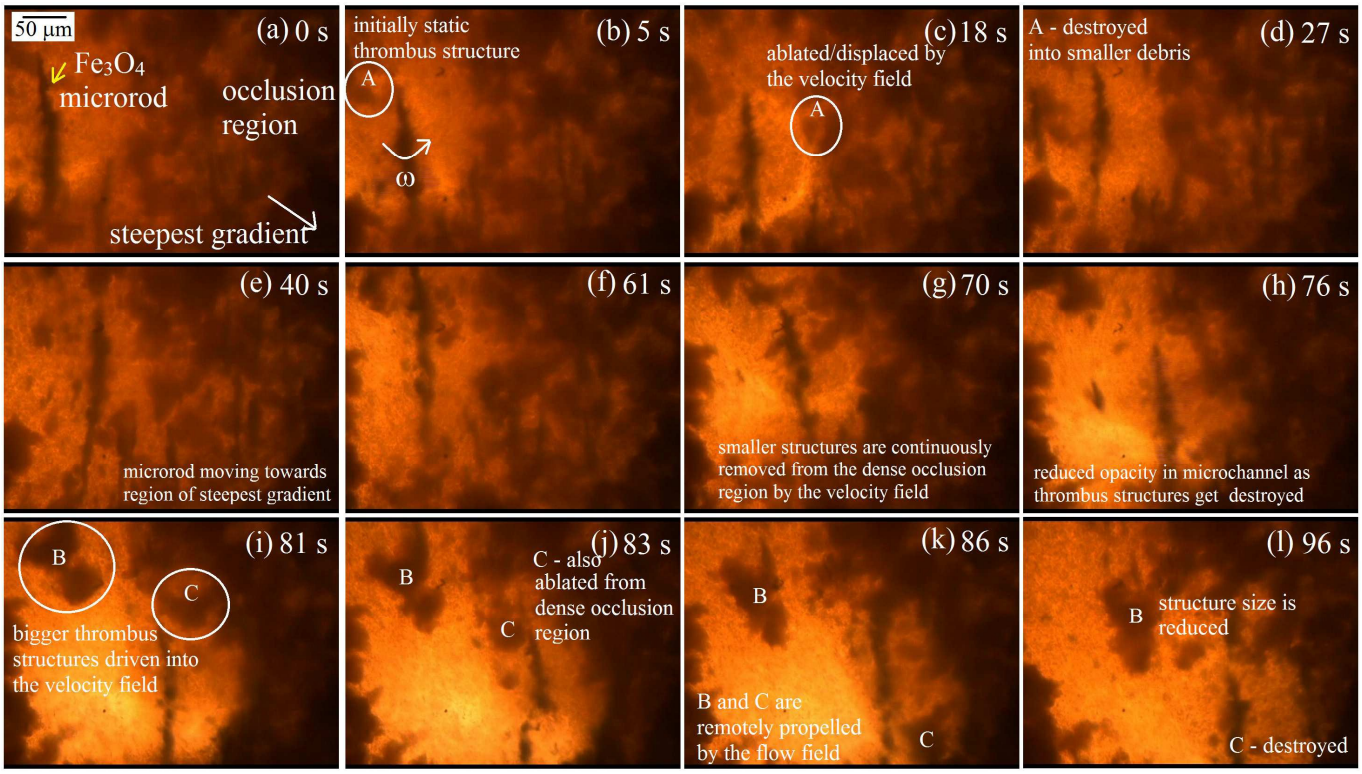

Fig. 5 Image sequence demonstrating the non-contact removal of microchannel occlusion (thrombus) recorded at higher magnification (100x). A microrod (length of ~200 μm) with its long axis aligned to a static magnetic field is rotating towards the direction of the steepest magnetic field gradient. The rotational flow field generated by such rotation creates a velocity flow field, which acts as a lift mechanism to remove the occlusion. *(See corresponding ESI Video S3)*

Conclusions

An oscillating magnetic field-driven manipulation system which exploits the agglomeration of Fe_3O_4 nanoparticles for non-contact removal of occlusions (thrombus or blood clot) in a microchannel was presented. We surmised that the rotation of microrods exposed to a weak oscillating magnetic field generates a hydrodynamic drag force as a result of the rotational flow field. The non-uniform velocity distribution of the fluid flow applies a lifting (drag) force, which destroys the occlusion. By steering Fe_3O_4 microrods along the magnetic field gradient, we demonstrated a technique for fast and non-contact thrombus ablation in a microchannel. As a new approach for microsurgery, we show that controlling the dimension of the microrods and their trajectory using an oscillating field source is promisingly simple and easily scalable in comparison to mechanical devices traditionally used for the same application.

Affiliations

[a] Center for Biomedical Technology, Chung Yuan Christian University, Zhongli City 32023, Taiwan.

[b] Mapua Institute of Technology, Intramuros, Manila 1002, Philippines. E-mail: jlfgabayno@mapua.edu.ph

[c] Department of Engineering, Chung Yuan Christian University, Zhongli City 32023, Taiwan. E-mail: ming@cycu.edu.tw

Acknowledgements

This research is supported by the Ministry of Science and Technology of Taiwan under grant No. 102-2218-E-033-002-MY2 and Chung Yuan Christian University. J. Gabayno also acknowledges the financial support from the Mapua Institute of Technology, Philippines.

Electronic Supplementary Material: Additional information of the magnetic properties of the Fe_3O_4 nanoparticles, setup configuration, and videos of thrombus removal process are available in the online version of this article at http://dx.doi.org/10.1007/s12274-***-****-* (automatically inserted by the publisher).

Notes

Materials. Fe_3O_4 nanopowders were purchased from Top Nano Technology Co. Ltd. Batch preparation was assisted by first rinsing the nanoparticles and then sonication in deionized (DI) water. Nanoparticles from the same batch were suspended in DI water and kept at room temperature. Bright field TEM images of the IONPs at different magnification are shown in ESI Fig. S1. The micrographs revealed that the nanoparticles have spherical morphology and relatively uniform size distribution. The calculated mean grain size of the nanoparticles was 50 nm.

The magnetic properties of the nanoparticles were measured using a superconducting quantum interference device (SQUID) magnetometer at room temperature. The magnetization (M-H) curve

in Fig. S1(c) depicts superparamagnetic behaviour with a very narrow hysteresis loop and coercivity of 3 Oe (Fig. S1d). The remanence magnetization was approximately zero and the magnetic saturation M_s was calculated at 55 emu/g.

Manipulation Device. The manipulation platform for the Fe_3O_4 nanoparticles consisted of a permanent and an oscillating magnet field source. The oscillating magnetic field was generated by a single solenoid connected to a variable-amplitude AC generator. Figure S2 shows the position of the magnetic field sources with respect to the Fe_3O_4 nanoparticle suspension. The permanent magnet was placed sufficiently close (2~4 cm) to the container. It can be moved along the x-y plane to orient the microrod axis to any direction. The remanent magnetic field of the bar magnet is 0.3 T. The copper solenoid was placed beneath the glass tank. It simultaneously provides the oscillating field to induce torque for rotation and the field gradient for microrod translation. A calibrated magnetometer was used to measure the magnetic field strength at the centre and rim of the tank for all the measurements.

Optical Tracking. A high-speed camera (X-Stream XS-3) attached to an optical microscope was used to track the motion of the microrods. Video recordings at 100x magnification were captured and loaded on a computer. The linear speed (v) of individual microrods was calculated by measuring the displacement divided by the time interval and then taking the average over the entire tracking period. The rotation (ω) speed was determined by tracking the period of one complete rotation. ESI Fig. S2b shows the SEM image of the microrods formed by the agglomeration of the nanoparticles. The magnetization vector is along the plane perpendicular to the microrod long axis. Figure S2 also shows the tracking positions of a microrod for different magnitude of the field gradient and oscillating magnetic field.

References

1 Q. A. Pankhurst, J. Connolly, S. K. Jones and J. Dobson, *J. Phys. D: Appl. Phys.*, 2003, **36**, R167-R181.
2 J. Wang and W. Gao, *ACS Nano*, 2012, **6**, 5745-5751.
3 K. E. Peyer, L. Zhang and B. Nelson, *Nanoscale,* 2013, **5**, 1259-1272.
4 X. Chao, Z. Zhang, L. Guo, J. Zhu, M. Peng, A. Vermoken, W. Van de Ven, C. Chen and Y. Cui, *PLoS One*, 2012, **7**, 1-7.
5 L. Zhang, T. Petit, K. E. Peyer and B. J. Nelson, *Nanomed-Nanotechnol.*, 2012, **8**, 1074-1080.
6 K. Woo, J. Hong, S. Choi, H. W. Lee, J. P. Ahn, C. S. Kim and S. W. Lee, *Chem. Mater.*, 2004, **16**, 2814-2818.
7 H. El Ghandoor, H. M. Zidan, M. M. H. Khalil and M. I. M. Ismail, *Int. J. Electochem. Sci.*, 2012, **7**, 5734-5745.
8 R. Snovski, J. Grinblat, M. T. Sougrati, J. C. Jumas and S. Margel, *J. Magn. Magn. Mater.*, 2013, **349**, 35-44.
9 A. H. Lu, E. L. Salabas and F. Schüth, *Angew. Chem. Int. Ed.*, 2007, **46**, 1222-1244.
10 A. K. Gupta and M. Gupta, *Biomaterials*, 2005, **26**, 3995-4021;
11 X. Chao, F. Shi, Y. Y. Zhao, K. Li, M. L. Peng, C. Chen and Y. L. Cui, *Pharmazie*, 2010, **65**, 500-504.
12 W. Wu, Q. He and C. Jiang, *Nanoscale Res. Lett.*, 2008, **3**, 397-415.
13 L. Soler, V. Magdanz, V. M. Fomin, S. Sanchez and O. G. Schmidt, *ACS Nano,* 2013, **7**, 9611-9620.
14 W. Gao, A. Pei and J. Wang, *ACS Nano,* 2012, **6**, 8432-8438.
15 W. Wang, L. A. Castro, M. Hoyos and T. E. Mallouk, *ACS Nano*, 2012, **6**, 6122-6132.
16 W. Wang, W. Duan, S. Ahmed, T. E. Mallouk and A. Sen, *Nano Today,* 2013, **8**, 531-554.
17 L. Baraban, R. Streubel, D. Makarov, L. Han, D. Karnaushenko, O. G. Schmidt and G. Cuniberti, *ACS Nano,* 2013, **7**, 1360-1367.
18 V. Gradilla, J. Orozco, S. Sattayasamitsathit, F. Soto, F. Kuralay, A. Pourazary, A. Katzenberg, W. Gao, Y. Shen and J. Wang, *ACS Nano*, 2013, **7**, 9232-9240.
19 R. S. M. Rikken, R. J. M. Nolte, J. C. Maan, J. C. M. van Hest, D. A. Wilson and P. C. M. Christianen, *Soft Matter*, 2014, **10**, 1295-1308.
20 L. Zhang, K. E. Peyer and B. J. Nelson, *Lab Chip*, 2010, **10**, 2203-2215.
21 D. L. Fan, F. Q. Zhu, R. C. Cammarata and C. L. Chien, *Phys. Rev. Lett.*, 2005, **94**, 247208.
22 T. Honda, K. I. Arai and K. Ishiyama, *IEEE Trans. Magn.*, 1996, **32**, 5085-5087.
23 A. Ghosh and P. Fischer, *Nano Lett.*, 2009, **9**, 2243-2245.
24 W. Gao, S. Sattayasamitsathit, K. M. Manesh, D. Weihs and J. Wang, *J. Am. Chem. Soc.*, 2010, **132**, 14403-14405.
25 O. S. Pak, W. Gao, J. Wang and E. Lauga, *Soft Matter*, 2011, **7**, 8169-8181.
26 I. S. M. Khalil, H. M. Dijkslag, L. Abelmann and S. Misra, *Appl. Phys. Lett.*, 2014, **104**, 223701.
27 J. S. Andreu, J. Camacho, J. Faraudo, M. Benelmekki, C. Rebollo and Ll. M. Martinez, *Phys. Rev. E*, 2011, **84**, 021402.
28 J. Faraudo, J. S. Anreu and J. Camacho, *Soft Matter*, 2013, **9**, 6654-6664.
29 J.K. Lim, S. P. Yeap, C. H. Leow, P. Y. Toh and S. C. Low, *J. Colloid Interface Sci.,* 2014, **421**, 170-177.
30 A. Hultgren, M. Tanase, C. S. Chen, G. J. Meyer and D. H. Reich, *J. Appl. Phys.*, 2003, **93**, 7554-7556.
31 A. T. Chwang and T. Y. Wu, *J. Fluid Mech.*, 1976, **63**, 607-622.
32 D. Letellier, O. Sandre, C. Meneger, V. Cabuil and M. Lavergne, *Mat. Sci. Eng. C,* 1997, **5**, 153-162.
33 O. Sandre, J. Browaeys, R. Perzynski, J.-C. Bacri, V. Cabuil and R. E. Rosensweig, *Phys. Rev. E*, 1999, **59**, 1736-1746.
34 J. J. Abbott, O. Ergeneman, M. P. Kummer, A. M. Hirt and B. J. Nelson, *IEEE T. Robotics*, 2007, **23**, 1247-1252.
35 E. Loth, *Powder Technol.*, 2008, **182**, 342-353.
36 E. Lauga and T. R. Powers, *Rep. Prog. Phys.*, 2009, **72**, 096601.
37 P. Cherukat and J. Mclaughlin, *J. Fluid Mech.*, 1994, **263**, 1-18.
38 E. Nierop, S. Luther, J. Bluemink, J. Magnaudet, A. Prosperetti and D. Lohse, *J. Fluid Mech.*, 2007, **571**, 439-454.
39 Z. Ye, E. Diller and M. Sitti, *J. Appl. Phys.*, 2012, **112**, 064912.
40 H.-W. Tung, K. E. Peyer, D. F. Sargent and B. J. Nelson, *App. Phys. Lett.*, 2013, **103**, 114101.
41 S. Sudo, S. Segawa and T. Honda, *J. Intell. Mater. Syst. Struct.,* 2006, **17**, 729-736.